# A Novel Heterocyclic Schiff Base: Electrochemical and Antioxidant Investigation

**Youcef Bellal[1,*], Meriem Hamoudi[2] and Samira Ghedjati[2]**

[1]*Research Centre in Industrial Technologies CRTI, Cheraga, Algiers, Algeria*
[2]*Laboratory of Phytotherapy Applied to Chronic Diseases, Faculty of Natural and Life Sciences, University Ferhat Abbas Setif, Setif, Algeria*
*Corresponding author: y.bellal@crti.dz /youcefbellal324@yahoo.fr

Received 19/03/2024; accepted 25/07/2024
https://doi.org/10.4152/pea.2026440204

**Abstract**
Electrochemical and AA study of a new heterocyclic Schiff base ($L_1$) was herein carried out for the first time. Electrochemical results and AA tests were performed using PDP, *in vitro*, by ABTS, $C_{40}H_{56}/C_{18}H_{32}O_2$, DPPH and FRAP, respectively. IE(%) of this compound against corrosion of MS, immersed in a KOH simulated concrete solution (pH of 13.5), with 0.8 M $Cl^-$, was investigated. Electrochemical results showed that $L_1$ was a good CI, even at low Ct (from $10^{-3}$ to $10^{-6}$ M; $\tau_{inhib} > 98\%$), the best scavenger in DPPH and ABTS ($IC_{50}$: 0.022 ± 0.00 and 0.003 ± 7.92E-05 µg/mL, respectively), and the most active in $C_{40}H_{56}/C_{18}H_{32}O_2$ test, with a an IE(%) of 80.22 ± 1.58%. $L_1$ exhibited a significant reducing capacity ($A_{0.5}$: 0.008 ± 0.00 mg/mL) analogous to that obtained for Trolox ($A_{0.5}$: 0.008 ± 9.14 05 mg/mL). This study demonstrated $L_1$ good IE(%) and AA.

***Keywords***: ABTS; AA; CI; DPPH; IE(%); $L_1$.

## Introduction•

Schiff bases have shown to possess medicinal and biological anticonvulsant, anti-inflammatory, anti-cancer, anti-bacterial, anti-microbial, anti-tubercular, anti-viral, anti-fungal, anti-HIV and anti-oxidant properties [1-10].

They are well-known as fabulous ligands, since the imine groups forming chelates with metal ions show a strong affinity with transition metal ions, making them very stable materials suitable for surface coating, catalysis and electro-catalysis [11-18].

Studies by [2-23] on unsymmetrical tetradentate $N_2O_2$ Schiff base complexes for biological activity, and CI of steel sheets, have revealed that, in a chlorinated basic medium simulating the pore water in concrete, the more higher the Ct of aggressive ions such as $Cl^-$, the stronger the CR [24-26].

The addition of Schiff's bases CI at different Ct remarkably decreases CR. Sometimes, the addition of small quantities of these compounds ($10^{-5}$-$10^{-6}$ M) improves CI [27, 28].

•The abbreviations list is in pages 133-134.

Schiff-base N,N-bis(2-furaldehyde)−1,3-diaminopropane and its complex with Fe have been prepared and used as CI for MS in a 3.5% NaCl medium artificial marine environment, to evaluate the functional groups' IE(%) [29]. Electrochemical measurements showed the inhibitors' significant resistance to charge transfer through the electrolyte–metal interface, and mixed-type behavior. Furthermore, the film formed onto the MS surface was examined by SEM [29].
Essential oil of *Thymus satureoides* and Octacalcium phosphate were studied as CI for stainless and carbon steels in a saline environment of 3% NaCl. The compounds had IE(%) of 82 and 93.1%, respectively. Examination of the metal surface contact morphology by SEM revealed the formation of a protective layer [30, 31].
Due to DPPH, ABTS and $C_{40}H_{56}$/$C_{18}H_{32}O_2$ bleaching and reducing properties, they have been the most widely used for assessing AA. AA is defined as the average free radical scavenging capacity, and it is measured using DPPH and ABTS, which are stable free radicals. AA is also evaluated by other methods based on different mechanisms of action, such as the ability to reduce and inhibit lipid peroxidation. $C_{40}H_{56}$ bleaching and $C_{18}H_{32}O_2$ test is one of the AA tests suitable for plant samples and other products. In this test, AA is determined by measuring the production inhibition of volatile organic compounds, and the formation of conjugated diene hydroperoxides resulting from the oxidation of $C_{18}H_{32}O_2$, which leads to the discoloration of $C_{40}H_{56}$.
The transformation of ferric Fe into ferrous FE has been determined as reduction capacity of compounds, which may indicate electron-donation activity, an important mechanism of AA, and it may be strongly correlated with other AA.
In a study by [32], three Schiff bases have been synthesized by condensation reaction of the same aminophenol in different positions (ortho/meta/para) with 2-hydroxy-3 methoxybenzaldehyde, of which biological properties have been assesses (scavenging of DPPH radical and $C_{40}H_{56}$ bleaching). The variable results showed on a certain degree of increasing inhibitory effects by the synthesized Schiff bases.
DPPH analysis shows its good IE(%) against the corrosion of MS reinforcements with concrete in 0.5 M NaCl, due to N and O atoms in the ligand structure, which are suitable sites for interaction between this compound and the MS surface, in the CI process [27, 28].
The present work aimed to investigate the IE(%) and AA of an original synthesized Schiff base ($L_1$) *vs.* rebar corrosion in NaCl. First, $L_1$ structure was synthesized and determined by XRD [27]. Then, electrochemical proprieties were examined employing PDP technique. Finally, AA, by DPPH, ABTS, $C_{40}H_{56}$/$C_{18}H_{32}O_2$ and FRAP tests, was investigated.

## Materials and methods

### *Schiff base ($L_1$) synthesis*

$L_1$ was synthesized through a condensation reaction of 1 mmol/159.19 mg and 1 mmol/168.15 mg 3-amino-2-naphthol and DHA, respectively (Scheme 1) [27].

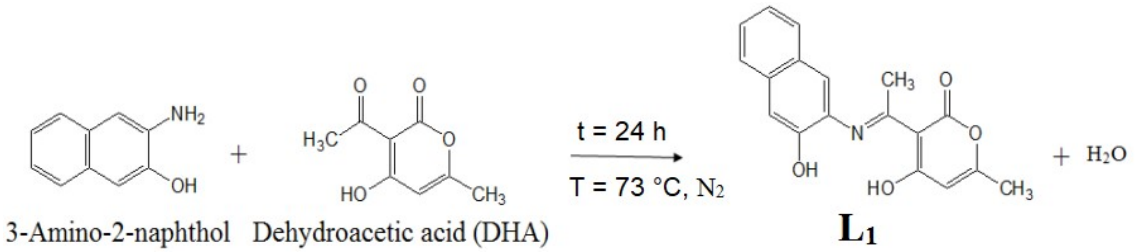


**Scheme 1:** Synthesized $L_1$.

### *$L_1$ characterization*

*Crystal structure characterization*

X-RD intensities for $L_1$ were assessed at the University of Strasbourg, France. The data were collected at 173(2) K, on a Collect diffractometer (Nonius BV, 1998), up to a graphic monochromator, using a fine-focus Mo K α sealed tube as radiation source, and employing phi and omega scan method. $L_1$ structure was solved and refined by SHELXS-97 program (Sheldrick, 1997) [33].

### *Electrochemical study*

The electrochemical study was carried out using PGSTAT309N (Autolab Potentiostat/Galvanostat). The three-electrode system was comprised by GCE as WE, Pt plate (S = 10 $mm^2$) as AE, and SCE ($Hg/Hg_2Cl_2/KCl$) as RE. NOVA Software Switzerland piloted by Pc was used to analyse experimental results. The GCE surface was polished with wet SiC paper of size 350-2000, rinsed with acetone, and then with distilled water. GCE was placed individually in the electrolytes (0.1 M KOH and DMSO), with $10^{-6}$ M $L_1$ and without it.

Before starting and recording polarization curves, OCP was maintained for 30 min, until it reached a steady state. Firstly, the cathodic branch was recorded. Then, the anodic branch was determined after establishing OCP. Potential sweep rate was 5 $mV/s^{-1}$. Electrochemical tests were carried out at room T of 25 ºC.

CI behaviour of $L_1$ was examined using a VOLTA- LAB PGZ 301, MS coated with parafilm, as WE, a Pt plate (S = 10 $mm^2$) as AE, and Hg/HgO system as RE. Voltamaster 4 software was employed to analyse experimental results.

Before starting and recording polarization curves, OCP was assured for each plot of polarization curves, during 30 min. For the three electrode systems in the different solutions, the potential became stable. At this moment, the stability potential value was taken and added to the polarization curves plot, and Tafel parameters ($I_{corr}$ and $E_{corr}$) were determined. At first, the cathodic branch was recorded. Then, the anodic branch was determined, after establishing OCP. Potential sweep rate was 10 $mV/s^{-1}$.

### *AA*

*DPPH radical scavenging assay*

Free radical scavenging activity of extracts against stable DPPH was determined using the method described by [34]. 0.5 mL samples were added to a 1 mL 0.1 mM DPPH solution. The mixture was strongly shaken and left to

stand at room T, for 30 min. The samples' changes in color (from deep-violet to light yellow) and absorbance were measured at 517 nm. Radical scavenging activity (%) was calculated using Eq. (1):

$$\text{Radical scavenging activity (\%)} = [A_{control} - A_{sample}] / A_{control} \times 100 \quad (1)$$

where $A_{control}$ is the absorbance of the control reaction (containing all reagents, except the sample) and $A_{sample}$ is the product absorbance.
A curve of IE(%) or scavenging effect against the sample Ct was plotted. Then, the sample Ct required for 50% IE(%) was determined. The value for each test sample was presented as the IE(%) curve at 50% or $IC_{50}$.

*ABTS free radical scavenging ability*
Free radical scavenging activity was determined by ABTS decolorization study by [35]. It was generated by a reaction of 7 mM ABTS with 2.45 mM $K_2S_2O_8$. The reaction mixture was allowed to stand in the dark for 16 h, at room T. The solution was then diluted by mixing ABTS with $CH_3OH$, to obtain an absorbance of 0.70 ± 0.02 units, at 734 nm. Then, 50 µl sample were mixed with 1 mL ABTS + solution, and kept for 30 min at room T. The reaction mixture absorbance was measured at 734 nm. ABTS scavenging capacity on the product was compared with that of QUER and BHT. IE(%) was calculated by Eq. (2):

$$\text{ABTS radical scavenging activity (\%)} = [(Ab_c - Ab_s) / (Abc)] \times 100 \quad (2)$$

where $Ab_c$ and $Ab_s$ are ABTS radical' $CH_3OH$ and sample/standard absorbance, respectively.

*$C_{40}H_{56}$ bleaching test*
In this test, the AA of the products was determined by measuring the inhibition of $C_{40}H_{56}$ oxidative decomposition (discoloration) by $C_{18}H_{32}O_2$ oxidation products, according to the method described by [36-38]. $C_{40}H_{56}/C_{18}H_{32}O_2$ emulsion was prepared by dissolving 0.5 mg $C_{40}H_{56}$ in 1 mL chloroform, to which 25 µl $C_{18}H_{32}O_2$ and 200 mg Tween 40 were added. Then, 100 mL distilled water saturated with O were added to the reaction mixture. 350 µl extract or BHT solubilized in 2 mg/mL $CH_3OH$ were mixed with 2.5 mL emulsion.
The same procedure was repeated with $CH_3OH$ and $H_2O$, as negative control. Absorbance was measured at 490 nm, after 1, 2, 3, 4, 6 and 24 h IT, at room T, in the dark. $C_{40}H_{56}$ decomposition (%) by the extract's AA was calculated by Eq. (3):

$$AA\% = ABS_{test} / ABS_{BHT} \times 100 \quad (3)$$

where AA% is AA percentage, and $ABS_{test}$ and $ABS_{BHT}$ are absorbance values without and with BHT, respectively.

Reducing power activity
The reducing power of the product was estimated according to the method described by [39]. 100 µl of the sample with various Ct were mixed with an equal volume of 0.2 M PBS (PH = 6.6) and 1% [$K_3Fe(CN_6)$]. The reaction was

incubated at 50 ºC, in a water bath, for 20 min, and it was terminated by the addition of 250 µl 10% $C_2HCl_3O_2$, followed by centrifugation, for 10 min, at 3000 rpm. 250 µl of the solution upper layer were mixed with 250 µl distilled water and 500 µl $FeCl_3$. The absorbance was measured at 700 nm against a blank. Stronger absorbance indicated higher reducing power. BHT, QUER and trolox were used as positive controls.

## Results and discussion

### *Characterization of $L_1$*

*X-RD description*

X-RD patterns extracted from CIF [27] confirm the presence of the polycrystalline phase of $L_1$ as monoclinic crystal structure, with preferential orientation along (110), (002), (200), (10-2), (011), (110), (102), (11-1), (210), (211), (212), (021), (121), (12-2) and (122) (Fig. 1).

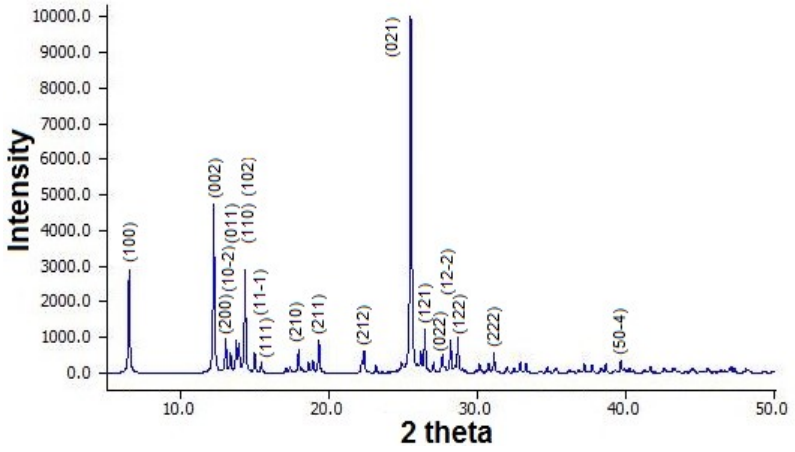


**Figure 1:** X-RD of $L_1$.

The same intense peaks that appeared at 2 theta = 12.26, 15.39 and 25.58 will only be characteristic peaks of 3-Amino-2-naphthol [28].

### *CV*

*Electrochemical study*

Electrochemical characteristics, such as $E_{corr}$, $i_{corr}$ and IE(%) are presented in Table 1.

**Table 1:** Electrochemical characteristics of GCE without and with $10^{-6}$ M $L_1$ in 0.1 M KOH and DMSO.

| Sample | I ($\mu A/cm^2$) | E (mV/SCE) | IE(%) |
|---|---|---|---|
| 0.1 M KOH | 1860.88 | -333.46 | |
| 0.1 M KOH + $N_2$ | 1115.2 | -239.86 | 40.07 |
| 0.1 M KOH + $10^{-6}$ M $L_1$ | 778.14 | -283.90 | 58.60 |
| 0.1 M KOH + $N_2$ + $10^{-6}$ M $L_1$ | 1188.97 | -283.83 | 36.10 |
| DMSO | 669.51 | -246.43 | 64.02 *vs.* 0.1 M KOH |
| DMSO + $10^{-6}$ M $L_1$ | 345.65 | -304.45 | 48.37 vs. DMSO |

IE(%) was obtained from Eq. (4):

$$EI(\%)=[(i_{corr}-i_{corr(inh)})/i_{corr}] \times 100 \quad (4)$$

where $i_{corr}$ and $i_{corr(inh)}$ are $i_{corr}$ values without and with inhibitor, respectively, obtained by intersecting $E_{corr}$, $\beta_a$ and $\beta_c$ lines (Fig. 2).

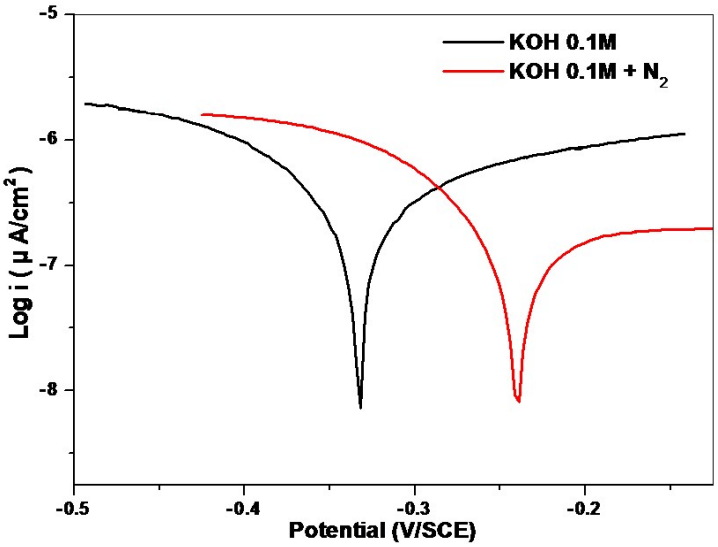


**Figure 2:** Tafel curves for GCE in 0.1 M KOH with and without $N_2$.

*$N_2$ gas effect*

In CV for GCE (Fig. 3), there was one positive reduction peak shift from -333.46 (0.1 M KOH) to -239.86 mV (0.1 M KOH + $N_2$), attributed to $O_2$ electrochemical reduction to $H_2O_2$ (reactions 5, 6 and 7) [40].

$$O_2 + e^- \rightarrow O_2^- \quad (5)$$

$$O_2^{\bullet-} + 2H^+ + e^- \rightarrow H_2O_2 \quad (6)$$

$$O_2 + 2H^+ + 2e^- \rightarrow H_2O_2 \quad (7)$$

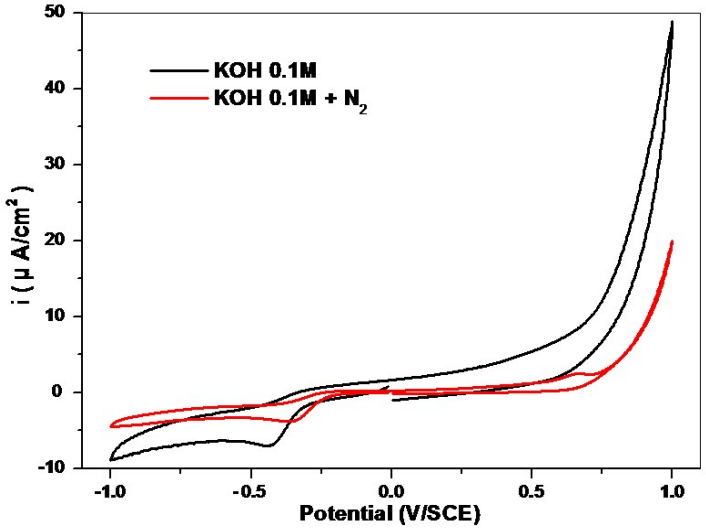


**Figure 3:** CV for GCE in 0.1 M KOH with and without $N_2$.

$I_{corr}$ decreased from 1860.88 to 1115.2 µA /cm$^2$ , for 0.1 M KOH and 0.1 M KOH + $N_2$, respectively (Table 2), due to $H^+$ consumption and reaction in the solution with O, which increased its basicity, and decreased the conductivity at the solution-electrode interface [41].

*$L_1$ effect*

$L_1$ addition (Figs. 4 and 5) led to a decrease in $i_{corr}$ and to a shift in $E_{corr}$ towards more positive values: -333.46 (0.1 M KOH) to 283.90 mV (0.1 M KOH + $10^{-6}$ M $L_1$), with an IE(%) of 58.60.

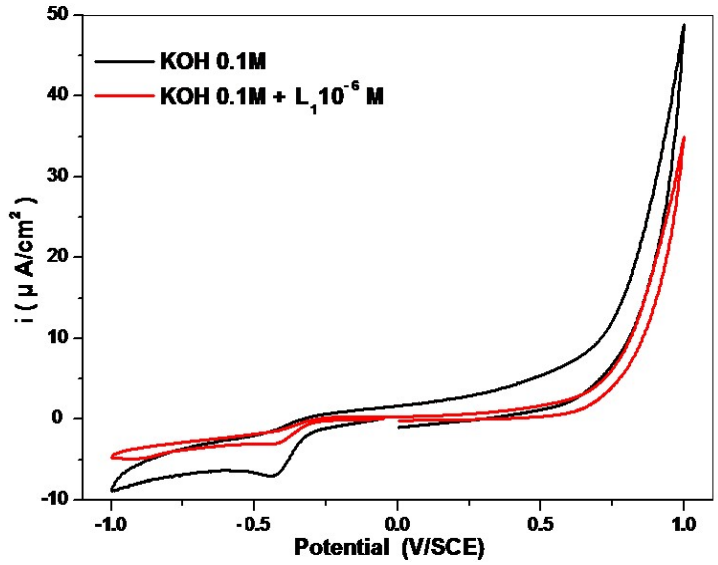


**Figure 4:** CV for GCE in 0.1 M KOH with and without $10^{-6}$ M $L_1$.

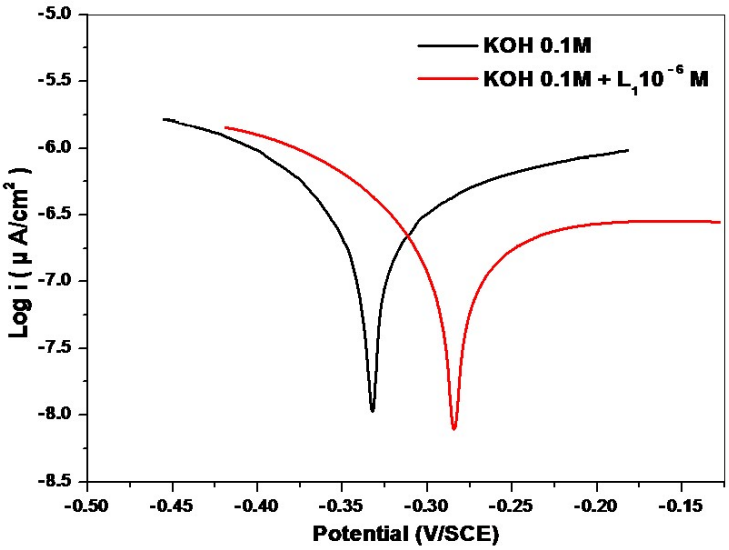


**Figure 5:** Tafel curves for GCE in 0.1 M KOH with and without $10^{-6}$ M $L_1$.

However, looking at CV and Tafel curves of GCE (Figs. 6 and 7), degassing with $N_2$ had no potential displacement influence, since $E_{corr}$ was -283.83 mV/SCE. However, it increased $i_{corr}$ and decreased IE(%) to 36.10.

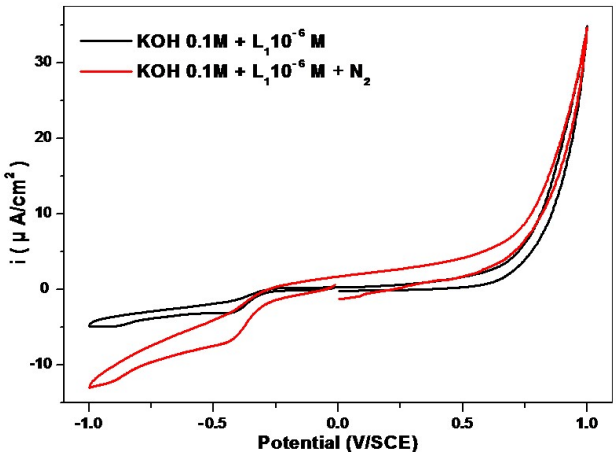


**Figure 6:** CV for GCE in 0.1 M KOH + $10^{-6}$ M $L_1$ with and without $N_2$.

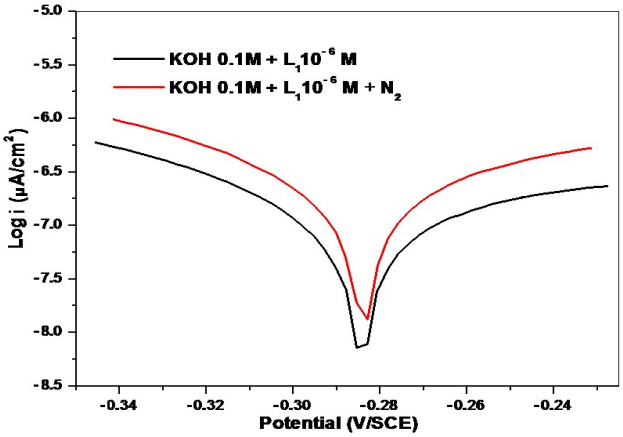


**Figure 7:** Tafel curves for GCE in 0.1 M KOH + $10^{-6}$ M $L_1$ with and without $N_2$.

*Solvent effect*

According to Table 2, GCE immersion in blank DMSO greatly decreased $i_{corr}$ and caused $E_{corr}$ shifts to positive values *vs.* 0.1 M KOH. $10^{-6}$ M $L_1$ addition decreased $i_{corr}$ even more (IE(%) = 48.37), with an $E_{corr}$ displacement to negative values *vs.* DMSO (Figs. 8 and 9).

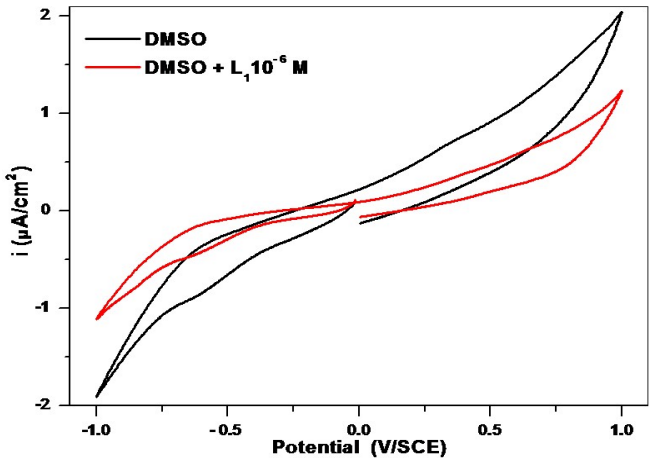


**Figure 8:** CV for GCE in DMSO with and without $10^{-6}$ M $L_1$.

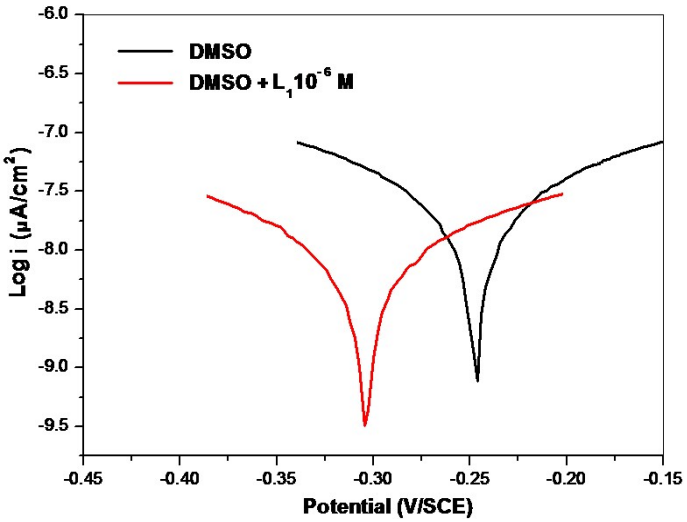


**Figure 9:** Tafel curves for GCE in DMSO with and without $10^{-6}$ M $L_1$.

### *Corrosion study*

$E_{corr}$ and $I_{corr}$ dissolution peaks for MS immersed in KOH (pH = 13.5) with 0.8 M NaCl, as a function of IT (0, 7, 14, 21 and 28 days), were assessed. WE were cylindrical MS rebars (Table 2) with 6 mm diameter and 28.26 $mm^2$ S.

Before each electrochemical test, the WE lower section was mechanical polished with SiC paper of different grain sizes, then with Al. The remaining electrodes were protected with Teflon, and each polishing was followed by rinsing with distilled water.

Throughout the study and after each test, the WE, RE and AE were cleaned with distilled water. The WE underwent the same polishing conditions, to have reproducible results.

**Table 2:** Rebar metal (chemical composition).

| Elements | Mn | Si | Cr | Mo | Ni | Sn | Cu | C | Fe |
|---|---|---|---|---|---|---|---|---|---|
| % | 0.423 | 0.58 | 0.079 | 0.029 | 0.215 | 0.013 | 0.536 | 0.804 | Remainder |

*Polarization curves without $L_1$*

PDP curves obtained by studying MS electrochemical behavior in 0.8 M $Cl^-$, as a function of IT (Fig. 10), showed that the corrosion peak became more intense.

The corrosion mechanism in the basic medium proceeded according to reactions (8-9) [42-47]:

$$\text{Anodic zone: } Fe \longrightarrow Fe^{2+} + 2e^- \quad (8)$$

$$\text{Cathodic zone: } 2H_2O + O_2 + 4\,e^- \longrightarrow 4OH^- \quad (9)$$

During the second stage of the corrosion process, the dissolved metal ion ($Fe^{2+}$) reacted with hydroxyls to form a precipitate which covered MS, following reaction (10):

$$Fe^{2+} + 2\,OH^- \longrightarrow Fe(OH)_2 \quad (10)$$

In solid concrete, i.e., if pH > 11, and in $Cl^-$ total absence, FeOOH protective layer formation is noted, following reaction (11):

$$Fe(OH)_2 \longrightarrow FeOOH + H^+ + e^- \quad (11)$$

In $Cl^-$ presence, the coating product no longer became waterproof, and MS corroded, according to reactions (12-15):

$$FeOOH + 3H^+ \longrightarrow Fe^{3+} + 2H_2O \quad (12)$$

$$Fe^{3+} + 3\ Cl^- \longrightarrow FeCl_3 \quad (13)$$

$$Fe + 3\ Cl^- \longrightarrow FeCl_3^- + 2e^-;\ (FeCl_3^-: \text{unstable complex}) \quad (14)$$

$$FeCl_3^- + 2\ OH^- \longrightarrow Fe(OH)_2 + 3\ Cl^- \quad (15)$$

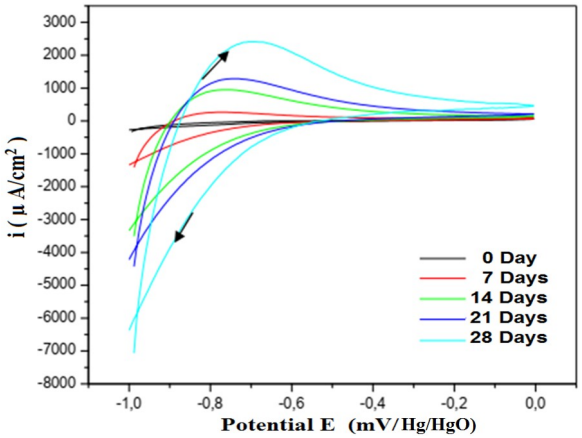


**Figure 10:** Polarization curves of MS in the presence of $Cl^-$ ions, as an IT function.

When the Ct of $Cl^-$ is lower than that of hydroxyl ions, stable $Fe(OH)_2$ formation occurs; if it is higher, formed $Fe(OH)_2$ is unstable, and green rust ([2 $Fe(OH)_2$, FeOHCl, $Fe(OH)_2$ Cl]), as an intermediate compound, is formed, which turns into lepidocrocite (hydrated ferric oxide ($Fe_2O_3$, $H_2O$)) containing chlorine, according to reaction (16):

$$2\ [\ 2\ Fe(OH)_2, FeOHCl\ ] \longrightarrow [\ 2\ Fe(OH)_2, FeOHCl, Fe(OH)_2\ Cl\ ] + Fe(OH)_2 + FeOH \quad (16)$$

Hydroxide II — Green rust I — Hydroxide I

The use of these curves and the plots of corresponding Tafel curves allowed to determine various electrochemical parameters ($E_{corr}$, $I_{corr}$, $R_p$ and CR). Table 3 shows a shift on $E_{corr}$ towards negative values, with an increase in CR and a decrease in $R_p$, as an IT function.

**Table 3:** Electrochemical parameters related to structural MS in a solution simulating concrete pore water of in $Cl^-$ presence.

| IT (days) | $E_{corr}$ (mV) | $i_{corr}$ (µA/cm²) | $R_p$ (k/Ohm/cm²) | CR (µm/an) |
|---|---|---|---|---|
| 0 | -636.4 | 11,45 | 18.66 | 133.8 |
| 7 | -890.4 | 127,00 | 0.24002 | 1485 |
| 14 | -904.1 | 336,60 | 0.07038 | 3937 |
| 21 | -891.4 | 485,30 | 0.05485 | 5676 |
| 28 | -879.1 | 710,90 | 0.03542 | 8315 |

*Polarization curves with $L_1$*

The analysis of polarization curves, obtained (Fig. 11) for MS immersed in a solution simulating concrete pore water with 0.8 M $Cl^-$ and different Ct of $L_1$, at an IT of 28 days, shows that the CI addition decreased $i_{corr}$.

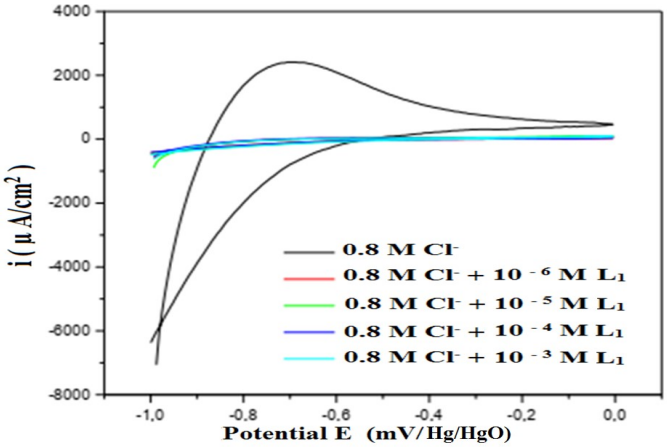


**Figure 11:** Polarization curves of MS with 0.8 M $Cl^-$ and different Ct of $L_1$.

These curvatures allowed drawing Tafel curves (Fig. 12), which show a shift in $E_{corr}$ towards less negative values, and a reduction in $i_{corr}$. The corresponding electrochemical parameters are grouped in Table 4.

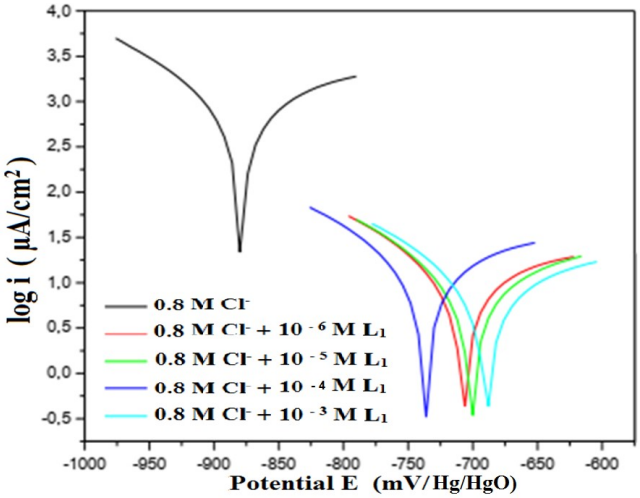


**Figure 12:** Tafel curves of MS in 0.8 M $Cl^-$ and different Ct of $L_1$.

**Table 4:** Electrochemical characteristics of MS in a solution simulating concrete pore water with $Cl^-$ and different Ct of $L_1$, for 28 days IT.

| Samples | $E_{corr}$ (mV) | $i_{corr}$ (µA/cm²) | $R_p$ (K/Ohm/cm²) | CR (µm/year) | IE(%) |
|---|---|---|---|---|---|
| 0.8 M $Cl^-$ | 879.1 | 710,90 | 0.03542 | 8315 | - |
| 0.8 M $Cl^-$ + $10^{-6}$ M $L_1$ | 706.0 | 8.90 | 3.19 | 104.1 | 98.74 |
| 0.8 M $Cl^-$ + $10^{-5}$ M $L_1$ | 699.8 | 8.52 | 3.31 | 99.75 | 98.8 |
| 0.8 M $Cl^-$ + $10^{-4}$ M $L_1$ | 735.8 | 12.99 | 2.28 | 151.9 | 98.17 |
| 0.8 M $Cl^-$ + $10^{-3}$ M $L_1$ | 688.0 | 8.06 | 3.73 | 94.34 | 98.86 |

The addition of various Ct of $L_1$ decreased CR of MS, as a function of IT (Table 5).

**Table 5:** Evolution of $i_{corr}$ ($\mu A/cm^2$) as IT functions, at different Ct of $L_1$ with 0.8 M $Cl^-$.

| Samples | $i_{corr}$ ($\mu A/cm^2$) | | | | |
|---|---|---|---|---|---|
| | 0 days | 7 days | 14 days | 21 days | 28 days |
| 0.8 M $Cl^-$ | 11.44 | 127.0 | 336.6 | 485.3 | 710.9 |
| 0.8 M $Cl^-$ + $10^{-6}$ M $L_1$ | 1.51 | 12.74 | 14.39 | 10.39 | 8.90 |
| 0.8 M $Cl^-$ + $10^{-5}$ M $L_1$ | 1.76 | 25.45 | 12.86 | 11.56 | 8.52 |
| 0.8 M $Cl^-$ + $10^{-4}$ M $L_1$ | 1.41 | 74.58 | 16.01 | 15.93 | 12.99 |
| 0.8 M $Cl^-$ + $10^{-3}$ M $L_1$ | 3.23 | 27.41 | 13.04 | 12.70 | 8.06 |

CR evolution of MS in a solution without and with different Ct of $L_1$, as a function of IT (Fig.13), shows that it is always lower than that of MS immersed in a solution with blank $Cl^-$.

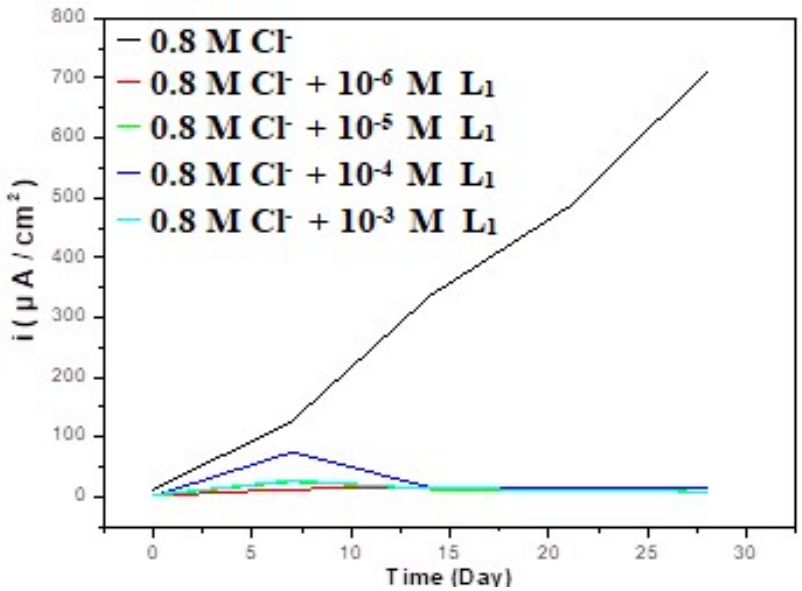


**Figure 13:** Development of CR for MS in 0.8 M $Cl^-$, at different Ct of $L_1$, as IT function.

The immediate addition of $L_1$ caused a significant inhibition (≥ 70%) which increases as a function of IT, with lower Ct. This confirms the $L_1$ inhibitory action by the creation of a protective film composed of an activated complex $[Fe_n(Cl)_p(L_2)_m]$ [28] which is responsible for blocking the of $Cl^-$ ions access to the MS/solution interface. Therefore, CI was enabled by the adsorption of this activated complex onto the active sites [28], due to the electron density of N and O unpaired electrons enhanced by naphthol group electrons.

***AA***

$L_1$ antiradical activity, which was given as $IC_{50}$ = 0.022 ± 0.003 µg/mL, was remarkable. Such activity was significantly higher than that of Trolox ($IC_{50}$ = 0.005 ± 2.985E-05 µg/mL) and QUER ($IC_{50}$ = 0.003 ± 5.248E-05 µg/mL) (Fig. 14).

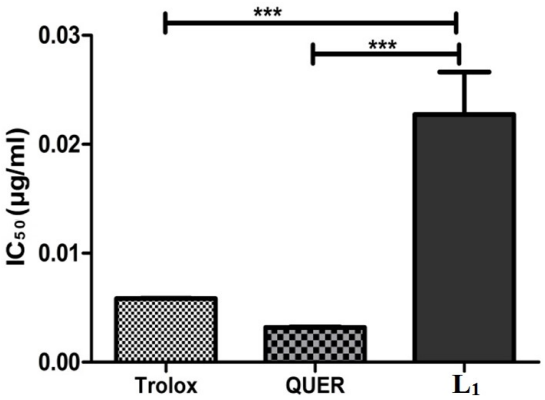


**Figure 14:** Scavenging activity of $L_1$ on DPPH radical. Data were presented as $IC_{50}$ means ± SD (n = 3); ***p < 0.001 were compared to Trolox and QUER as standards.

$L_1$'s scavenging activity was significantly higher than the one from Trolox ($IC_{50}$ = 0.005 ± 2.985E-05 µg/mL) and QUER ($IC_{50}$ = 0.003 ± 5.248E-05 µg/mL) (Fig. 15). The measurement of AA with DPPH and ABTS assays is rapid, sensitive, and more frequently applied for preliminary evaluation of various substances. Although the basic principles are similar, ABTS assay is preferable for assessing the activity of lipophilic and hydrophilic antioxidants [48-51]. In contrast, DPPH is more selective, because it does not react with flavonoids, which do not contain hydroxyl groups in B ring [52, 53].

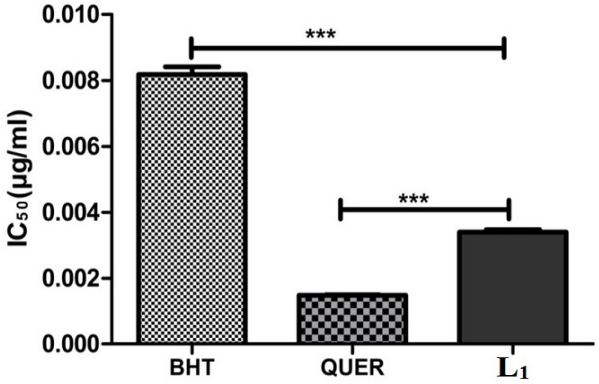


**Figure 15:** Scavenging activity of L1 on ABTS radical. Data were presented as IC50 means ± SD (n = 3); ***p < 0.001 was compared to BHT and QUER as standards.

According to the obtained results, a very important anti-lipid peroxidation activity was observed with $L_1$. Fig. 16 shows stronger AA (80.22 ± 1.585%) than that of synthetic BHT (100 ± 2.890%), at the same Ct.

This activity may be due to the nature of antioxidants that inhibit $C_{18}H_{32}O_2$ oxidation and neutralize free radicals, or simultaneously both [54-56]. A product that delays or inhibits $C_{40}H_{56}$ bleaching can be described as a free radical scavenger and as a primary antioxidant [57-59].

QUER, Trolox and BHT standard antioxidants showed potent reducing power with an $IC_{50}$ value of 0.002 ± 5.211E-05, 0.008 ± 9.142E-05 and 0.016 ± 0.000 µg/mL, respectively.

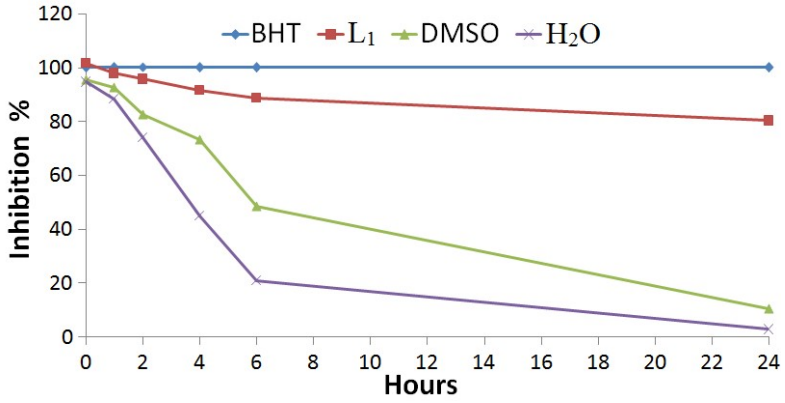


**Figure 16:** $L_1$ AA (2 mg/mL, at 24 h IT) was measured by $C_{40}H_{56}$ bleaching method. BHT was used as reference antioxidant. Values are mean ± SD (n = 3).

According to Fig. 17, $L_1$ has a strong reducing effect similar to Trolox, with $IC_{50}$ = 0.008 ± 0.000 µg/ mL, and moderate activity, in comparison with BHT and QUER.

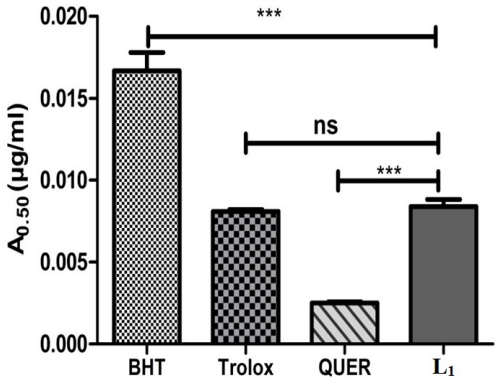


**Figure 17:** $L_1$ reducing power. Values are as absorbance means ± SD (n = 3). (ns: no significant difference. *** $p < 0.001$ was compared to BHT, Trolox and QUER, as standards.

This power is due to the presence of electron-donating compounds that can inhibit chain reactions triggered by free radicals, and reduce oxidized intermediates of lipid peroxidation processes [60-63]. $L_1$ was additionally stabilized by an intramolecular hydrogen bond with the ortho-phenolic group. Moreover, the introduction of donor substituents (-CH 3) to phenol hydroxyls is known to reduce the bond dissociation enthalpy of the O–H bond, thereby stimulating the hydrogen abstraction process [64]. The comparison of the Schiff base's AA with Trolox and QUER provides valuable insights into its effectiveness. It should be noted that AA of $L_1$ phenolic compound are mainly associated with their relatively high reactivity in hydrogen abstraction reactions. This circumstance may be explained by the stabilization of the formed phenoxyl radical by delocalization of the unpaired electron in an extended conjugated two aromatic systems. Enhancement of AA of $L_1$ is usually associated with the introduction of additional hydroxyl groups into their chemical structure, as well as with a decrease of sterical hindrance at the hydrogen abstraction site [65].

## Conclusion

In this paper, an original non-symmetrical tridentate Schiff base ($L_1$) was synthesized by a condensation reaction of an aldehyde and an amine, for electrochemical and biological study. This product was produced in a well-defined crystalline form.

The polarization curves, which were carried out using GCE as WE, showed the presence of reduction peaks, due to O reduction.

The inhibition study of MS, in a 0.8 M $Cl^-$ simulated solution of concrete water pores, obtained good results at diverse Ct of $L_1$, with a rate of around 98%. The *in vitro* AA was evaluated.

O and N were the atoms responsible for physicochemical interaction and AA. Thus, the density and morphology of this organic product may influence AA capacity.

$L_1$ was a best scavenger of ABTS than DPPH, and the most active in $C_{40}H_{56}/C_{18}H_{32}O_2$ test, with an inhibition percentage of 80.22%. The results showed that $L_1$ displayed an important reducing effect similar to that of Trolox. $L_1$ was additionally stabilized by an intramolecular hydrogen bond with the ortho-phenolic group. It should be noted that AA of $L_1$ phenolic compound is mainly associated with its relatively high reactivity in hydrogen abstraction reactions. This circumstance may be explained by the stabilization of the formed phenoxyl radical by delocalization of the unpaired electron in an extended conjugated two aromatic systems. Enhancement of AA of $L_1$ is usually associated with the introduction of additional hydroxyl groups into their chemical structure, and with a decrease of sterical hindrance at the hydrogen abstraction site.

## Acknowledgments

The authors gratefully acknowledge the support of the Directorate General for Scientific Research and Technological Development (DGRSDT) of Algeria, and Mr. Fateh Mayouf from Research Center in Industrial Technologies, for his help.

## Authors' contributions

**Youcef Bellal**: conceptualized ideas; wrote the paper; review and editing; synthesis and caracterization; methodology; voltammetry experiment; analyzed data; interpretation; corresponding author. **Meriem Hamoudi**: biological experiment; interpretation; developed some sections of the manuscript. **Samira Ghedjati**: biological experiment; interpretation; developed some sections of the manuscript.

## Abbreviations

**AA**: antioxidant activity
**ABTS**: ethylbenzothiazoline-6-sulfonic acid/$C_{18}H_{18}N_4O_6S_4$
**AE**: auxiliary electrode
$\beta_a$: Tafel's anodic slope
$\beta_c$: Tafel's cathodic slope
**BHT**: butylated hydroxytoluene

**$C_2HCl_3O_2$**: trichloroacetic acid
**$C_{18}H_{32}O_2$**: linoleic acid
**$C_{40}H_{56}$**: β-carotene
**$CH_3OH$**: methanol
**CI**: corrosion inhibition/inhibitor
**CIF**: crystallographic information file
**CR**: corrosion rate
**Ct**: concentration
**CV**: cyclic voltammetry
**DHA**: dehydroacetic acid
**DMSO**: dimethyl sulfoxide
**DPPH**: 2,2-diphenyl-1-picrylhydrazyl/$C_{18}H_{12}N_5O_6$
**$E_{corr}$**: corrosion potential
**$FeCl_3$**: iron (III) chloride
**$Fe(OH)_2$**: iron hydroxide
**FeOOH**: iron(III) oxide-hydroxide
**FRAP**: ferric reducing antioxidant power
**GCE**: glassy carbon electrode
**$H_2O_2$**: hydrogen peroxide
**$Hg_2Cl_2$**: mercury(I) chloride
**$i_{corr}$**: corrosion current density
**IE(%)**: inhibition efficiency
**IT**: immersion time
**$K_2S_2O_8$**: potassium persulfate
**$[K_3Fe(CN_6)]$**: potassium ferricyanide
**KCl**: potassium chloride
**KOH**: potassium hydroxide
**$L_1$**: 4-hydroxy-3-[1-(3-hydroxy-naphthalene-2-ylimino)-ethyl]-6-methyl-pyran-2-one
**MS**: mild steel
**NaCl**: sodium chloride
**OCP**: open circuit potential
**PBS**: phosphate buffer solution
**PDP**: potentiodynamic polarization
**QUER**: quercetin
**RE**: reference electrode
**$R_p$**: polarization resistance
**Rpm**: rotation per minute
**SCE**: saturated calomel electrode
**SD**: standard deviation
**SEM**: scanning electron microscope
**SiC**: silicon carbide
**T**: temperature
**WE**: working electrode
**XRD**: X-ray diffraction

## References


1. Yakan H. Novel Schiff bases derived from Isothiocyanates: synthesis, characterization, and antioxidant activity. Res Chem Intermed. 2020;46:3979-3995. https://doi.org/10.1007/s11164-020-04185-w
2. Chen Y, Mi Y, Li Q et al. Synthesis of Schiff bases modified inulin derivatives for potential antifungal and antioxidant applications. Intern J Bio Macromol. 2020;143:714-723. https://doi.org/10.1016/j.ijbiomac.2019.09.127
3. Abd El-Halim HFA, Mohamed GG, Anwar MN. Antimicrobial and anticancer activities of Schiff base ligand and its transition metal mixed ligand complexes with heterocyclic base. Appl Organometal Chem. 2018;32:e3899. https://doi.org/10.1002/aoc.3899
4. Biradar SB, Narte DV, Kale RP et al. Synthesis, Spectral and Biological Studies of DHA Schiff Bases. J Appl Organomet Chem. 2021;1. https://doi.org/10.22034/jaoc.2021.275758.1003
5. Chemchem M, Menacer R, Merabet N et al. Green synthesis, antibacterial evaluation and QSAR analysis of some Isatin Schiff bases. J Molec Struc. 2020;1208:127853. https://doi.org/10.1016/j.molstruc.2020.127853
6. Gümüş A, Okumuş V, Gümüş S. Synthesis, biological evaluation of antioxidant-antibacterial activities and computational studies of novel anthracene- and pyrene-based Schiff base derivatives. Turk J Chem. 2020;44:1200-1215. https://doi.org/10.3906/kim-2005-61
7. Hassan A, Askar A, Nossier E et al. Antibacterial Evaluation, in Silico Characters and Molecular Docking of Schiff Bases Derived from 5-aminopyrazoles. Molecules. 2019;24:3130. https://doi.org/10.3390/molecules24173130
8. Magd-El-Din AA, Mousa HA, Labib AA et al. Benzimidazole – Schiff bases and their complexes: synthesis, anticancer activity and molecular modeling as *Aurora* kinase inhibitor. Zeitschr Naturforsch C. 2018;73(11-12):465-478. https://doi.org/10.1515/znc-2018-0010
9. Mishra N, Kumar K, Pandey H et al. Synthesis, characterization, optical and anti-bacterial properties of benzothiazole Schiff bases and their lanthanide (III) complexes. J Saud Chem Soc. 2020;24:925-933. https://doi.org/10.1016/j.jscs.2020.09.009
10. Rosato A, Catalano A, Carocci A et al. *In vitro* interactions between *Anidulafungin* and nonsteroidal anti-inflammatory drugs on biofilms of *Candida spp*. Bioorg Medic Chem. 2016;24:1002-1005. https://doi.org/10.1016/j.bmc.2016.01.026
11. Belbacha W, Naamoune F, Bezzi H et al. Elaboration of carbon paste electrode containing pentadentate Nickel-(II) Schiff base complex: Application to electrochemical oxidation of thiosulfate in alkaline medium. Arab J Chem. 2020;13:6072-6083. https://doi.org/10.1016/j.arabjc.2020.05.007
12. Bezza A, Ouennoughi Y, Bouzerafa B et al. New quaternized poly(4-vinylpyridine-co-divinylbenzene) material containing nickel(II) Schiff base complex: synthesis, thermogravimetry, and application for heterogeneous electrooxidation of ethanol. Res Chem Intermed. 2018;44:6831-6846. https://doi.org/10.1007/s11164-018-3524-8

13. Ghosh S, Roy N, Singh TS et al. Photophysics of a Coumarin based Schiff base in solvents of varying polarities. Spectrochim Acta A: Molec Biomolec Spectrosc. 2018;188:252-257. https://doi.org/10.1016/j.saa.2017.07.006
14. Maghraoui N, Aggoun D, Bouzerafa B et al. Synthesis, characterization, thermal stability, electrochemical behavior, and antioxidant activity of new oxovanadium(iv) and iron(ii) tetradentate Schiff base complexes. Arab J Chem. 2021;14:103025. https://doi.org/10.1016/j.arabjc.2021.103025
15. Ourari A, Nora H, Noureddine C et al. Elaboration of new electrodes with carbon paste containing polystyrene functionalized by pentadentate nickel(II)-Schiff base complex – Application to the electrooxidation reaction of methanol and its aliphatic analogs. Electrochim Acta. 2015;170:311-320. https://doi.org/10.1016/j.electacta.2015.02.154
16. Boudiaf M, Messai Y, Bentouhami E et al. Green synthesis of NiO nanoparticles using *Nigella sativa* extract and their enhanced electro-catalytic activity for the 4-nitrophenol degradation. J Phys Chem Sol. 2021;153:110020. https://doi.org/10.1016/j.jpcs.2021.110020
17. Xia L, Xia Y-F, Huang L-R et al. Benzaldehyde Schiff bases regulation to the metabolism, hemolysis, and virulence genes expression *In vitro* and their structure–microbicidal activity relationship. Euro J Medic Chem. 2015;97:83-93. https://doi.org/10.1016/j.ejmech.2015.04.042
18. Youcef M, Hamza B, Nora H et al. A novel green synthesized NiO nanoparticles modified glassy carbon electrode for non-enzymatic glucose sensing. Microchem J. 2022;178:107332. https://doi.org/10.1016/j.microc.2022.107332
19. Alturiqi AS, Alaghaz A-NA, Zayed ME et al. Synthesis, characterization, biological activity, and corrosion inhibition in acid medium of unsymmetrical tetradentate $N_2O_2$ Schiff base complexes. J Chin Chem Soc. 2018;65:1060-1074. https://doi.org/10.1002/jccs.201800027
20. Belaid S, Benali-Baïtich O, Bout G et al. Synthesis, characterization, and biological activities of oxovanadium(IV) and cadmium(II) complexes with reduced Schiff bases derived from N,N′-o-phenylenebis(salicylideneimine). Chem Pap. 2015;69(10). https://doi.org/10.1515/chempap-2015-0132
21. Boudjellal F, Ouici HB, Guendouzi A et al. Experimental and theoretical approach to the corrosion inhibition of mild steel in acid medium by a newly synthesized pyrazole carbothioamide heterocycle. J Molec Struc. 2020;199:127051. https://doi.org/10.1016/j.molstruc.2019.127051
22. Kaabi I, Douadi T, Daoud D et al. A New Synthesized Schiff Base as Corrosion Inhibitor for Mild Steel in a HCl Medium: Experimental, Density Functional Theory and Molecular Dynamics Simulation Studies. Port Electrochim Acta. 2021;39(05):349-379. https://doi.org/10.4152/pea.2021390504
23. Sehmi A, Ouici HB, Guendouzi A et al. Corrosion Inhibition of Mild Steel by newly Synthesized Pyrazole Carboxamide Derivatives in HCl Acid Medium: Experimental and Theoretical Studies. J Electrochem Soc. 2020;167:155508. https://doi.org/10.1149/1945-7111/abab25

24. Mennucci MM, Banczek EP, Rodrigues PRP et al. Evaluation of benzotriazole as corrosion inhibitor for carbon steel in simulated pore solution. Cem Concr Compos. 2009;31:418-424. https://doi.org/10.1016/j.cemconcomp.2009.04.005
25. Sail L, Benbrahim A. Comparative behavior study of steel corrosion inhibition kinetics by three phosphate inhibitors with mass loss measurements. J Adhes Sci Technol. 2020;34:48-66. https://doi.org/10.1080/01694243.2019.1660505
26. Khadraoui MHM, Obot IB, Sorrour A et al. Performance evaluation of a natural and synthetic compound as corrosion inhibitors of API 5L X52 steel in hydrochloric acid media. Mor J Chem. 2018;6(1):51-61. https://doi.org/10.48317/Imist.Prsm/Morjchem-V6I1.8608
27. Bellal Y, Keraghel S, Benghanem F et al. A New Inhibitor for Steel Rebar Corrosion in Concrete: Electrochemical and Theoretical Studies. Int J Electrochem Sci. 2018;13(7):7218-7245. https://doi.org/10.20964/2018.07.91
28. Bellal Y, Benghanem F, Keraghel S. A new corrosion inhibitor for steel rebar in concrete: Synthesis, electrochemical and theoretical studies. J Molec Struc. 2021;1225:129257. https://doi.org/10.1016/j.molstruc.2020.129257
29. Abdel HRS, El-Azabawy OE, El-Segaey AA et al. Comparison between Schiff-base and its iron complex as steel corrosion inhibitors used by the petroleum industry in marine environments. Canad Metallur Quart. 2023;63(1):1-13. https://doi.org/10.1080/00084433.2023.2268493
30. Simescu-Lazar F, Slaoui S, Essahli M et al. *Thymus satureoides* oil as green corrosion inhibitor for 316L stainless steel in 3% NaCl: Experimental and theoretical studies. Lubricants. 2023;11(2):56. https://doi.org/10.3390/lubricants11020056
31. Ferraa N, Ouakki M, El Harmouchi H et al. Investigation of the inhibition behavior of an octacalcium phosphate as a green corrosion inhibitor against carbon steel in 3% NaCl medium. Inorg Chem Commun. 2023;157:111343. https://doi.org/10.1016/j.inoche.2023.111343
32. Yekhlef R, Benghanem F, Foudia M et al. Synthesis, Spectroscopic and Thermal Characterization and Antioxidant Activities of Three Schiff Bases Derived from Aminophenol. Inter J Heat Technol. 2023;41(2):351-359. https://doi.org/10.18280/ijht.410208
33. Sheldrick GM. A short history of *SHELX*. Acta Crystallogr. 2008;64:112-122. https://doi.org/10.1107/S0108767307043930
34. Yardpiroon B. Phytochemical and Biological Activities of the Wild Grape Fruit Extracts Using Different Solvents. Brit J Pharm Res. 2014;4(1):23-36. https://doi.org/10.9734/BJPR/2014/5626
35. Bouaziz A, Khennouf S, Zarga MA et al. Phytochemical analysis, hypotensive effect and anti-oxidant activity of *Myrtus communis L*. growing in Algeria. Asi Pacif J Trop Biomed. 2015;5:19-28. https://doi.org/10.1016/S2221-1691(15)30165-9

36. Hamoudi M, Amroun D, Khennouf S et al. Antioxidant Evaluation and Polyphenol Contents of Hydro Ethanolic Extract's Fractions from *Ephedra nebrodensis*. J Drug Deliv Ther. 2020;10:314-319. https://doi.org/10.22270/jddt.v10i5-s.4377
37. Du Z, Wang D, Li Y. Comprehensive Evaluation and Comparison of Machine Learning Methods in QSAR Modeling of Antioxidant Tripeptides. ACS Omega. 2022;7:25760-25771. https://doi.org/10.1021/acsomega.2c03062
38. Munteanu IG, Apetrei C. Analytical Methods Used in Determining Antioxidant Activity: A Review. Inter J Molec Sci. 2021;22:3380. https://doi.org/10.3390/ijms22073380
39. Hamoudi M, Amroun D, Boutefnouchet S et al. Phytochemical Screening, *in vitro* Antioxidant and Enzyme Inhibitory Properties, and Acute Toxicity of Extracts from the Aerial Parts of *Ephedra nebrodensis*, a Source of Bioactive Compounds. Comb Chem High Throu Screen. 2022;25:1058-1071. https://doi.org/10.2174/1386207324666210303094339
40. Sadiek IM, Mohammad AM, El-Shakre ME et al. Enhanced electrolytic generation of oxygen gas at binary nickel oxide–cobalt oxide nanoparticle-modified electrodes. J Solid State Electrochem. 2013;17:871-879. https://doi.org/10.1007/s10008-012-1938-6
41. Ghavami N, Park CH, Kim CS. In Situ Synthesis of Antimicrobial Silver Nanoparticles within Antifouling Zwitterionic Hydrogels by Catecholic Redox Chemistry for Wound Healing Application. Biomacromolecules. 2016;17:1213-1223. https://doi.org/10.1021/acs.biomac.6b00039
42. Bhardwaj N, Sharma P, Kumar V. Phytochemicals as steel corrosion inhibitor: an insight into mechanism. Corros Rev. 2021;39:27-41. https://doi.org/10.1515/corrrev-2020-0046
43. Gromboni MF, Sales A, Rezende de AM et al. Impact of agro-industrial waste on steel corrosion susceptibility in media simulating concrete pore solutions. J Clean Prod. 2021;284:124697. https://doi.org/10.1016/j.jclepro.2020.124697
44. Landolt D. Corrosion et chimie de surfaces des métaux, Réimpr. Corr., Presses Polytechniques et Universitaires Romandes, Lausanne, 2003.
45. Chen S, Zhang D. Corrosion behavior of Q235 carbon steel in air-saturated seawater containing *Thalassospira sp*. Corros Sci. 2019;148:71-82. https://doi.org/10.1016/j.corsci.2018.11.031
46. Padash R, Rahimi-Nasrabadi M, Shokuhi RAS, et al. A theoretical study of two novel Schiff bases as inhibitors of carbon steel corrosion in acidic medium. App Phys. A. 2019;125:78. https://doi.org/10.1007/s00339-018-2376-9
47. Vorobyova V, Skiba M. Peach Pomace Extract as Efficient Sustainable Inhibitor for Carbon Steel Against Chloride-Induced Corrosion. J Bio Tribo Corros. 2021;7:11. https://doi.org/10.1007/s40735-020-00450-y
48. Dobravalskytė D, Venskutonis PR, Talou T. anti-oxidant properties and essential oil composition of *Calamintha grandiflora* L. Food Chem. 2012;135:1539-1546. https://doi.org/10.1016/j.foodchem.2012.05.094

49. Rodríguez-Bonilla P, Gandía-Herrero F, Matencio A et al. Comparative Study of the Antioxidant Capacity of Four Stilbenes Using ORAC, ABTS+, and FRAP Techniques. Food Analyt Meth. 2017;10:2994-3000. https://doi.org/10.1007/s12161-017-0871-9
50. Sozen E, Karademir B, Ozer NK. Basic mechanisms in endoplasmic reticulum stress and relation to cardiovascular diseases. Free Rad Biol Med. 2015;78:30-41. https://doi.org/10.1016/j.freeradbiomed.2014.09.031
51. Sridhar K, Charles AL. *In vitro* antioxidant activity of *Kyoho* grape extracts in DPPH and ABTS assays: Estimation methods for EC50 using advanced statistical programs. Food Chem. 2019;275:41-49. https://doi.org/10.1016/j.foodchem.2018.09.040
52. Yokozawa T, Chen CP, Dong E et al. Study on the Inhibitory Effect of Tannins and Flavonoids against the 1,1-Diphenyl-2-picrylhydrazyl Radical. Biochem Pharmacology. 1998;56:213-222. https://doi.org/10.1016/S0006-2952(98)00128-2
53. López CM, Piñeiro AE, Núñez N et al. Thyroid hormone changes in males exposed to lead in the Buenos Aires area (Argentina). Pharmac Res. 2000;42:599-602. https://doi.org/10.1006/phrs.2000.0734
54. Naidu MM, Shyamala BN, Naik JP et al. Chemical composition and antioxidant activity of the husk and endosperm of fenugreek seeds. LWT - Food Sci Technol. 2011;44:451-456. https://doi.org/10.1016/j.lwt.2010.08.013
55. Kim H-S, Ham S-Y, Jang Y et al. Linoleic acid, a plant fatty acid, controls membrane biofouling via inhibition of biofilm formation. Fuel. 2019;253:754-761. https://doi.org/10.1016/j.fuel.2019.05.064
56. Zimmer B, Angioni C, Osthues T et al. The oxidized linoleic acid metabolite 12,13-DiHOME mediates thermal hyperalgesia during inflammatory pain. Biochim Biophys Acta. 2018;1863:669-678. https://doi.org/10.1016/j.bbalip.2018.03.012
57. Loucif K, Benabdallah H, Benchikh F et al. Total Phenolic Contents, DPPH Radical Scavenging and β-Carotene Bleaching Activities of Aqueous Extract from *Ammoides atlantica*. J Drug Deliv Ther. 2020;10:196-198. https://doi.org/10.22270/jddt.v10i3-s.4151
58. Ahmed D, Malik W, Maqsood M et al. Study of anti-diabetic, beta-carotene-bleaching inhibiting and iron chelating properties of *Carissa opaca* root extracts. Braz J Pharm Sci. 2022;58:e18628. https://doi.org/10.1590/s2175-97902019000318628
59. Benabdallah A, Boumendjel M, Aissi O et al. Chemical composition, antioxidant activity and acetylcholinesterase inhibitory of wild *Mentha* species from northeastern Algeria. South Afr J Bot. 2018;116:131-139. https://doi.org/10.1016/j.sajb.2018.03.002
60. Djenidi H, Khennouf S, Bouaziz A. Antioxidant activity and phenolic content of commonly consumed fruits and vegetables in Algeria. Progr Nutr. 2020;22:224-235. https://doi.org/10.23751/pn.v22i1.7701

61. Khither H, Sobhi W, Khenchouche A et al. In-vitro Antioxidant Effect of Thymoquinone. Ann Res Rev Biol. 2018;25:1-9. https://doi.org/10.9734/ARRB/2018/40165
62. Merghem M, Dahamna S. In-Vitro Antioxidant Activity and Total Phenolic Content of *Ruta montana* L. Extracts. J Drug Delivery Ther. 2020;10:69-75. https://doi.org/10.22270/jddt.v10i2.3919
63. Muthuvel A, Jothibas M, Manoharan C. Synthesis of copper oxide nanoparticles by chemical and biogenic methods: photocatalytic degradation and *in vitro* antioxidant activity. Nanotechnol Environ Eng. 2020;5:14. https://doi.org/10.1007/s41204-020-00078-w
64. Lien EJ, Ren S, Bui HH et al. Quantitative structure-activity relationship analysis of phenolic antioxidants. Free Rad Biol Med. 1999;26(3-4):285-294. https://doi.org/10.1016/S0891-5849(98)00190-7
65. Augustyniak A, Bartosz G, Čipak A et al. Natural and synthetic antioxidants: an updated overview. Free Rad Res. 2010;44(10):1216-1262. https://doi.org/10.3109/10715762.2010.508495